Metal-insulator transition and ferromagnetism phenomena in $La_{0.7}Ce_{0.3}MnO_3$ thin films: Formation of Ce-rich nanoclusters

Takeshi Yanagida,[1] Teruo Kanki,[1] Bertrand Vilquin,[1] Hidekazu Tanaka,[1,2] and Tomoji Kawai[1,*]
[1]*Institute of Scientific and Industrial Research, Osaka University, 8-1 Mihogaoka, Ibaraki, Osaka 567-0047, Japan*
[2]*PRESTO, Japan Science and Technology Agency, 4-1-8 Honcho, Kawaguchi, Saitama 332-0012, Japan*
(Received 17 February 2004; revised manuscript received 10 August 2004; published 29 November 2004)

The nature of metal-insulator transition and ferromagnetism phenomena of perovskite $La_{0.7}Ce_{0.3}MnO_3$ thin films was investigated. In particular, the effects of post-annealing under oxidization and reduction atmospheres on the electrical transport and magnetic properties were systematically examined. The metal-insulator transition temperature and the Curie temperature of ferromagnetism were found to be significantly influenced by the post-annealing and increase with increasing the post-annealing temperature under both oxygen and argon atmospheres. In addition, the major carriers within the conductive films were identified to be holes. Structural and composition analysis clarified that cation deficiencies due to nanoclustering cerium oxides within the post-annealed films are responsible for the emergence of the metal-insulator transition and ferromagnetism phenomena.

DOI: 10.1103/PhysRevB.70.184437 PACS number(s): 75.70.Ak, 71.30.+h, 75.30.Kz

I. INTRODUCTION

Manganese perovskite oxides ($La_{1-x}A_xMnO_3$) exhibit a rich variety of electric transport and magnetic properties including colossal magnetoresistance (CMR) phenomena due to the strong coupling between spin, charge, and orbital degrees of freedom. Although numerous investigations in this field have been extensively reported, the major interest has been directed at hole-doped systems, in which the rare earth in the parent compound is partially replaced by a divalent cation such as Ba, Ca, Sr, and others—e.g., Refs. 1–9. As to the hole doping with the parent compound $LaMnO_3$, a proportionate amount of Mn^{3+} with electric configuration of $t_{2g}^3e_g^1$ is substituted with Mn^{4+} resulting in holes on the e_g band. On the other hand, electron-doped systems with doping a tetravalent cation including Ce,[10–16] Sn,[17–19] and others,[20,21] in which the valence state of Mn should be a mixed-valence state of Mn^{3+} and Mn^{2+}, have not been well examined compared with the hole-doped systems. If such electron-doped systems were available, the *p-n* homojunctions of both hole- and electron-doped systems will be possible and promising for novel functional spintronics devices in future.

Mandal and Das[10] first reported that Ce-doped $LaMnO_3$ bulk systems show paramagnetic-ferromagnetic transition and metal-insulator transition phenomena. Although they assumed the Ce-doped $LaMnO_3$ bulk systems to be electron-doped systems with the mixed-valence state of Mn^{3+} and Mn^{2+}, Philips and Kutty[22] demonstrated that the Ce-doped $LaMnO_3$ bulk systems showed hole-like behavior on the thermopower data. Later, Ganguly *et al.*[23] implicated that a lanthanum deficiency within Ce-doped $LaMnO_3$ bulk systems, which form a multiphase mixture comprising hole-doped lanthanum-deficient lanthanum manganate phases and cerium oxides, is responsible for the emergence of the metal-insulator (MI) transition and ferromagnetism (FM) phenomena.

As to the thin film systems, Mitra *et al.*[12] and Raychaudhuri *et al.*[14] reported that it is possible to fabricate a single phase of Ce-doped $LaMnO_3$ thin films without impurity phases of cerium oxides using a pulsed laser deposition (PLD) method. Joseph Joly *et al.*[24] claimed the lack of experimental evidence to prove whether their thin films indeed contain Ce. Later Mitra *et al.*[16] showed the experimental evidence to prove the existences of (i) Ce^{4+} and (ii) the mixed-valence state of Mn^{3+} and Mn^{2+} within their films by performing x-ray absorption spectroscopy. On the contrary, Zhao *et al.*[25] implicated the difficulty of the doping of Ce ions into $LaMnO_3$ systems, showing a significant peak due to CeO_2 impurity phases in the x-ray diffraction (XRD) data of their films. More importantly, their thermopower measurement indicated their Ce-doped $LaMnO_3$ films to be hole-doped systems.[25] There are obviously contradictive implications in the context with whether Ce-doped $LaMnO_3$ thin film systems can be intrinsically electron-doped systems.

In this paper, we report on the metal-insulator transition and ferromagnetic phenomena of $La_{0.7}Ce_{0.3}MnO_3$ thin films and their nature. Since a post-annealing plays an important role on the properties of hole-doped manganese oxides,[26] the post-annealing effect on the electric transport and magnetic properties of Ce-doped $LaMnO_3$ thin films was systematically investigated. The nature and origin of the phase transition phenomena were rigorously studied by performing microstructural and composition analysis. We found that *A*-site cation deficiencies due to nanoclustering cerium oxides are responsible for the metal-insulator transition and ferromagnetic phenomena of $La_{0.7}Ce_{0.3}MnO_3$ thin films.

II. EXPERIMENTAL DETAILS

Bulk samples were prepared by the conventional solid-state reaction route. La_2O_3, Mn_2O_3, and CeO_2 powders were mixed in mill for 2 h. Prior to the mixing, La_2O_3 powder was preheated at 800 °C for 72 h to evaporate a moisture within the powder. The mixed samples were then calcined at 800 °C for 20 h and reground for 2 h. Subsequently, the samples were sintered at 1350 °C for 20 h.

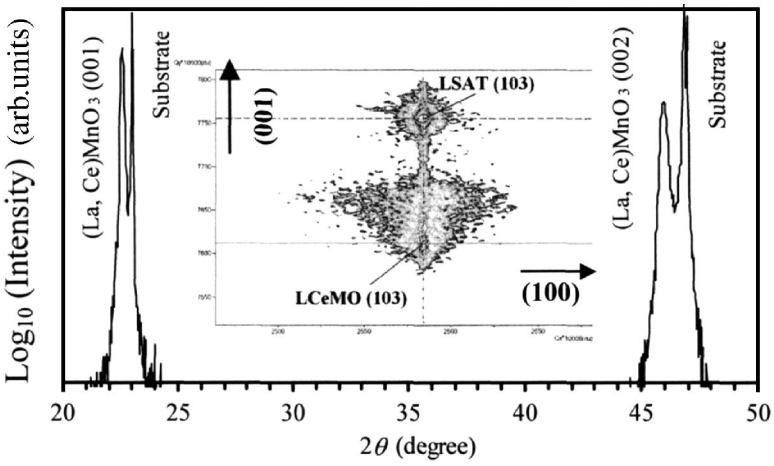

FIG. 1. Typical XRD pattern of as-grown $La_{0.7}Ce_{0.3}MnO_3$ thin film deposited on LSAT substrate. The inset shows the reciprocal map space measurement performed around the (103) peak.

The $La_{0.7}Ce_{0.3}MnO_3$ epitaxial films were fabricated by the PLD technique (ArF excimer, $\lambda = 193$ nm). These films were grown on either LSAT $[(LaAlO_3)_{0.3}(Sr_2AlTaO_6)_{0.7}]$ (001) ($d = 3.868$ Å) or STO $[SrTiO_3]$ (001) ($d = 3.905$ Å) single-crystal substrates in an oxygen atmosphere. The thickness of the films fabricated was controlled to be 1000 Å. The oxygen pressure P_{O_2} and the substrate temperature T_s during depositions were set to be 1 Pa and 700 °C, respectively.[27] The deposited films were then post-annealed at temperatures ranging from 500 to 800 °C in either flowing oxygen or argon at atmospheric pressure for 10 h.

The crystal structures of resultant films were characterized by XRD measurement and high-resolution transmission electron microscopy (HRTEM) coupled with electron diffraction (ED). The film composition was evaluated by electron probe microanalyzer (EPMA) coupled with energy dispersion spectroscopy (EDS) using the ZAF method. The electrical transport properties were measured by a four-probe method, and the magnetic properties were evaluated by a superconducting quantum interference device (SQUID).

III. RESULTS AND DISCUSSION

A. Transport and magnetic properties

The typical XRD data of $La_{0.7}Ce_{0.3}MnO_3$ thin films grown on LSAT substrate are shown in Fig. 1. The epitaxy of the film can be clearly seen, and more importantly there appeared no significant impurity peaks. Such well-epitaxial films are comparable to those of previous reports.[12–16] Figure 2 shows the temperature dependence of resistivity with various post-annealing temperatures under both oxygen and argon atmospheres. The as-grown films exhibited semiconductivelike behavior, but not a metal-insulator transition peak, which indeed differs from previous data.[12–16] When increasing the post-annealing temperature, the metal-insulator transition peak emerged and the transition temperature T_{MI} systematically increased. This was found for both oxygen and argon atmosphere post-annealing, indicating that the emergence of the metal-insulator transition phenomena cannot be attributable to only oxygen content changes within films during post-annealing. In addition, the post-annealing affected significantly ferromagnetism as shown in Fig. 3. In a similar manner to T_{MI}, the Curie temperature T_c increased with increasing the post-annealing temperature as seen in Fig. 4. The correlation between the post-annealing temperature dependences of both T_{MI} and T_c was also confirmed. As the post-annealing temperature increased from 500 to 800 °C, the phase transition temperatures were ranged from 150 to 300 K, which covers the transition temperature (250 K) reported previously.[12–16] There is a discrepancy between our results and previous reports on the appearance of a metal-

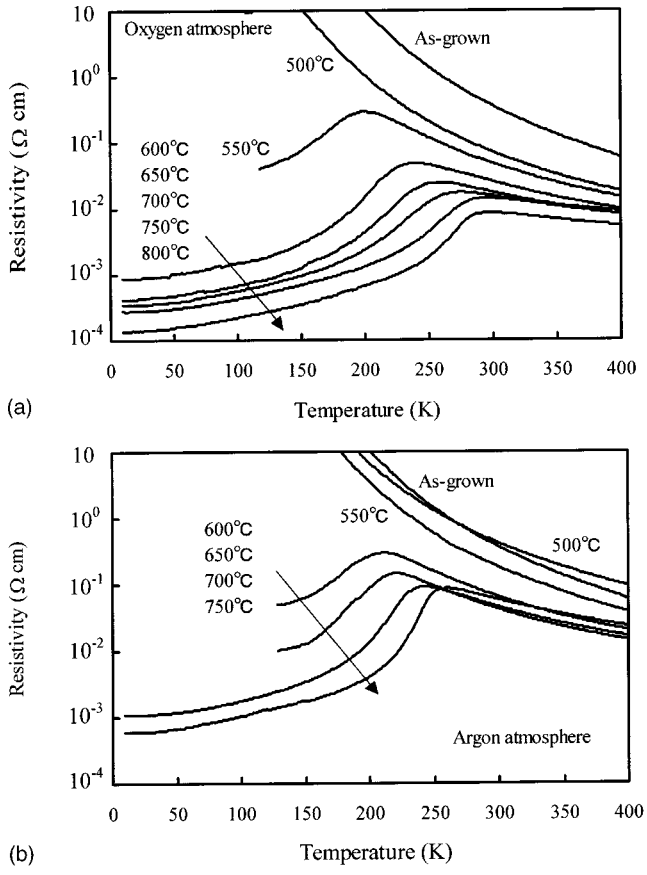

FIG. 2. (a) Effect of post-annealing temperature under oxygen atmosphere on the temperature dependence of resistivity. (b) Effect of post-annealing temperature under argon atmosphere on the temperature dependence of resistivity.

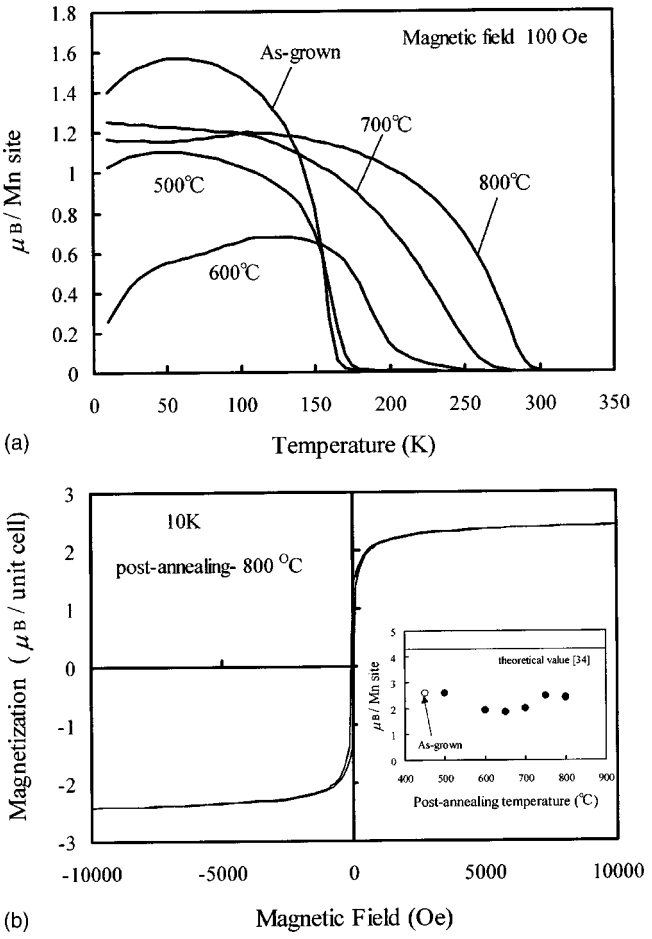

FIG. 3. (a) Effect of post-annealing temperature under oxygen atmosphere on the temperature dependence of magnetization. The measurements were performed at 100 Oe of magnetic field. (b) Magnetization versus magnetic field of post-annealed film at 800 °C under oxygen atmosphere. The measurement was performed at 10 K.

insulator transition for as grown films. Note that our deposition conditions are more reduction atmosphere compared with deposition conditions of previous reports (typically, 30–40 Pa of oxygen pressure, 700–800 °C of substrate

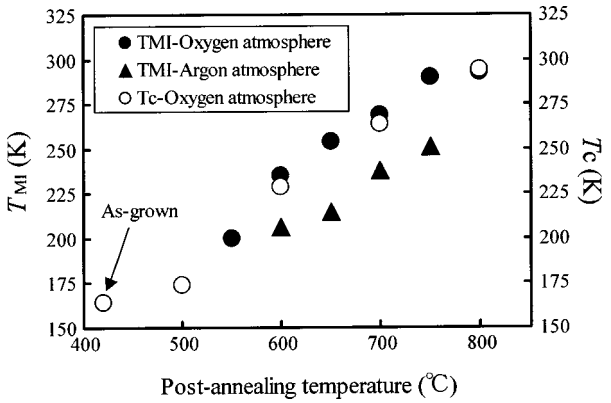

FIG. 4. (a) Post-annealing temperature dependences of the metal-insulator transition temperature. (b) Post-annealing temperature dependences of the Curie temperature.

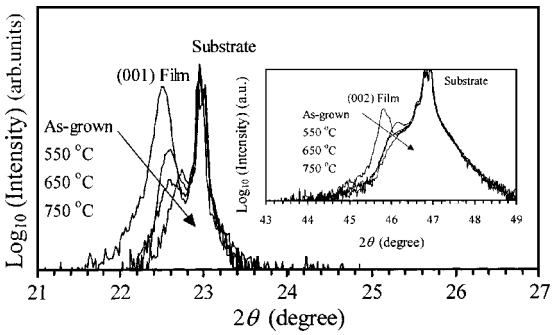

FIG. 5. Post-annealing temperature dependence under argon atmosphere on XRD data.

temperature).[12–16,25] It seems that our experiments essentially cover the range of such over oxidized films by performing post-annealing under oxygen atmosphere, in which the metal-insulator transition emerged. Considering the absence of impurity peaks on XRD data and the transition temperature range, it is believed that results of post-annealed films are considered to be comparable with previous reports. However, it remains for further investigation to examine the properties of such overoxidized films in the as-grown state without post-annealing. Figure 5 shows the post-annealing temperature dependence on both (001) and (002) diffraction peaks of (La,Ce)MnO_3 films. These diffraction peaks tended to be broader as the post-annealing temperature increased. At the post-annealing temperature of 750 °C, the (002) diffraction peak was hidden behind the substrate peak because the lattice constant tended to be smaller. Although the crystal structures were surely changed due to the post-annealing, further detailed microscopic information was not available from the XRD data. Thus microstructural TEM analysis would be essential and is performed in a later discussion. The above experimental results highlight that the post-annealing plays a crucial role on the phase transition phenomena including the metal-insulator and paramagnetic-ferromagnetic transition phenomena. As far as we are aware, none of the previous investigations has reported the significance of the post-annealing on Ce-doped $LaMnO_3$ systems, and therefore the nature of such effects is also unknown.

There seem to be three possible scenarios to interpret the emergence of the phase transition phenomena in our system. The first ideal scenario is based on a double-exchange interaction mechanism between Mn^{2+} and Mn^{3+} in which the system is an electron-doped system with electric configuration $t_{2g}^3 e_g^2$ (Refs. 12–16). The second scenario is based on *A*-site cation-deficient compositions of $(La,Ce)_\delta MnO_3$ with a significant change of the film composition during post-annealing. The phenomenon is actually quite similar to well-known La-deficient compositions of $La_{1-x}MnO_3$ systems.[28–30] The third possible scenario is based on nano-clustering cerium oxides, which results in a mixture of *A*-site cation-deficient compositions $(La,Ce_{1-\delta})MnO_3$ and CeO_2 phases, in which the entire film composition is maintained to be constant during post-annealing. It should be noted that the second and third scenarios assume the Ce-doped $LaMnO_3$ systems to be hole-doped systems.

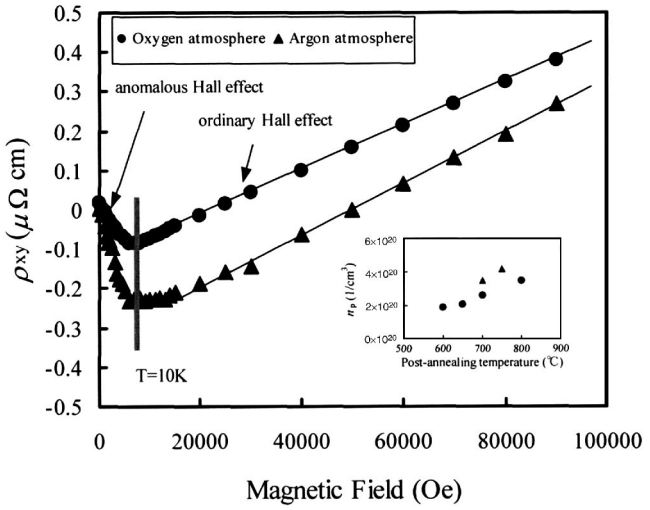

FIG. 6. Hall resistivity of $La_{0.7}Ce_{0.3}MnO_3$ thin film post-annealed under oxygen and argon atmospheres. The inset shows carrier concentrations of post-annealed films as a function of post-annealing temperature.

B. Hall measurement

Hall measurements were conducted in order to identify the type of major carriers within the films. Although the physical picture of Hall effect in strongly correlated systems, including anomalous Hall effect, is complex, it is possible to identify the carrier type in terms of the ordinary Hall effect at low temperature as reported elsewhere for manganites.[31–33] The measurements were performed at 10 K, well below the Curie temperatures, because an anomalous Hall effect rather than an ordinary Hall effect tends to be dominant near the Curie temperature.[31–33] The Hall resistivity of ferromagnetic materials can be described as the formula $\rho_{xy}=\mu_0 H R_0 + \mu_0 R_s M$. Here R_0 is the ordinary Hall coefficient, R_s the anomalous Hall coefficient, and μ_0 the vacuum permeability. In terms of the above formula, the Hall resistivity below T_c might be decomposed into the first ordinary Hall effect term ($\mu_0 H R_0$) and the second anomalous Hall effect term ($\mu_0 R_s M$), which shows a strong temperature dependence. Our intention herein is to identify the type of major carriers in terms of the ordinary Hall effects rather than to investigate the anomalous Hall effects. Figure 6 shows the typical Hall resistivity data of post-annealed thin films. All post-annealed samples showed a negative low-field slope due to the anomalous Hall effect and a positive high-field slope corresponding to the ordinary Hall effect. The positive high-field slope identified the major carriers within the post-annealed films to be holes. Note that the Hall measurements were not feasible for as-grown films because their resistivity at low temperatures was too high to perform Hall measurements. Adapting the simple case in the presence of only one type of carrier ($R_0=1/ne$), the effective "Hall density" n_p can be estimated and is shown in the inset of Fig. 6 as a function of the post-annealing temperature. n_p increased from 2.0×10^{20} to 3.5×10^{20} 1/m^3 with increasing the post-annealing temperature from 500 to 800 °C, indicating that the post-annealing temperature dependence of the film properties (see Figs. 2–4) can be reasonably interpreted in terms of doping holes. These Hall measurement results dismiss the first scenario based on the double-exchange interaction mechanism between Mn^{2+} and Mn^{3+} to explain the phase transition phenomena of our Ce-doped $LaMnO_3$ systems.

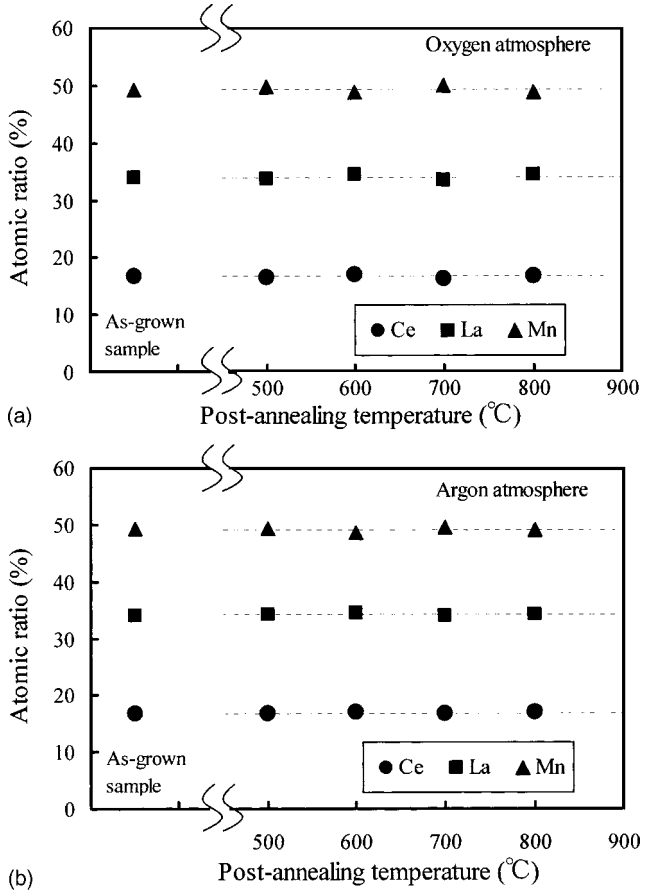

FIG. 7. (a) Effect of post-annealing temperature on cation concentrations within the post-annealed films under oxygen atmosphere. (b) Effect of post-annealing temperature on cation concentrations within the post-annealed films under argon atmosphere.

C. Composition analysis

Energy dissipative spectroscopy measurements were performed to detect change of the film composition during post-annealing. The films were deposited onto STO substrates in order to exclude the effect from substrate. Figure 7 shows the atomic cation ratio with varying post-annealing temperature. The nominal atomic cation ratio for $La_{0.7}Ce_{0.3}MnO_3$ systems is La:Mn:Ce=35:15:50. It was found that the post-annealing does not change significantly the atomic cation ratio within films, which indeed contradicts the assumption of the second scenario based on *A*-site cation-deficient compositions $(La,Ce)_\delta MnO_3$. It is noted that the EDS data cannot give intimate information as to microscopic inhomogeneity of the film composition since the measurements were performed on a relatively large scale over at least a submicron level.

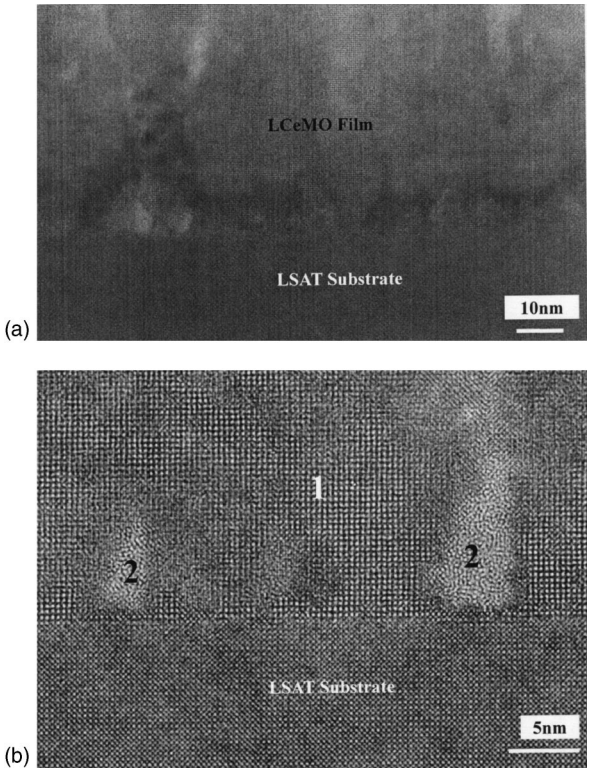

FIG. 8. High-resolution TEM image of as-grown $La_{0.7}Ce_{0.3}MnO_3$ thin film deposited on LSAT substrate.

D. Microstructural analysis

High-resolution transmission electron microscope analyses were performed to observe and compare the microstructures of both "as-grown" and "post-annealed" films. Figure 8 shows the HRTEM images of as-grown films. Well-crystallized film structure with the lattice fringes (point 1) can be clearly seen in the images, and amorphouslike nanoclusters (point 2) were found. The structural difference between the two phases was also confirmed in terms of electron diffraction patterns as shown in Fig. 9. Microscopic EDS analysis was performed with 1 nm of the electron beam spot size to detect the composition difference between the two phases. Figure 10 shows the EDS data of each phase. Although both phases were found to contain La, Mn, and Ce atoms, quantitative analysis of these data indicated the significant difference between the atomic cation ratios of the two phases—see Table I. The nanocluster phase was a Ce-rich and Mn-less phase compared to the well-crystallized phase by about 5%. Figure 11 shows the HRTEM image of film post-annealed at 800 °C under an oxygen atmosphere. When comparing with as-grown samples, clear changes in the structures of the post-annealed samples can be easily seen. There appeared three distinguished phases, which are marked as points 3–5 on the image. The ED patterns of the three phases are shown in Fig. 12. Point 3 is the primary phase, and the crystal structure was identified to be similar to point 1 in Fig. 8, which is perovskite structure. Point 4 has a crystal structure dissimilar to point 3, which can be obviously seen in the ED patterns. In addition, these diffraction patterns were assigned to CeO_2 crystal structures. Judging

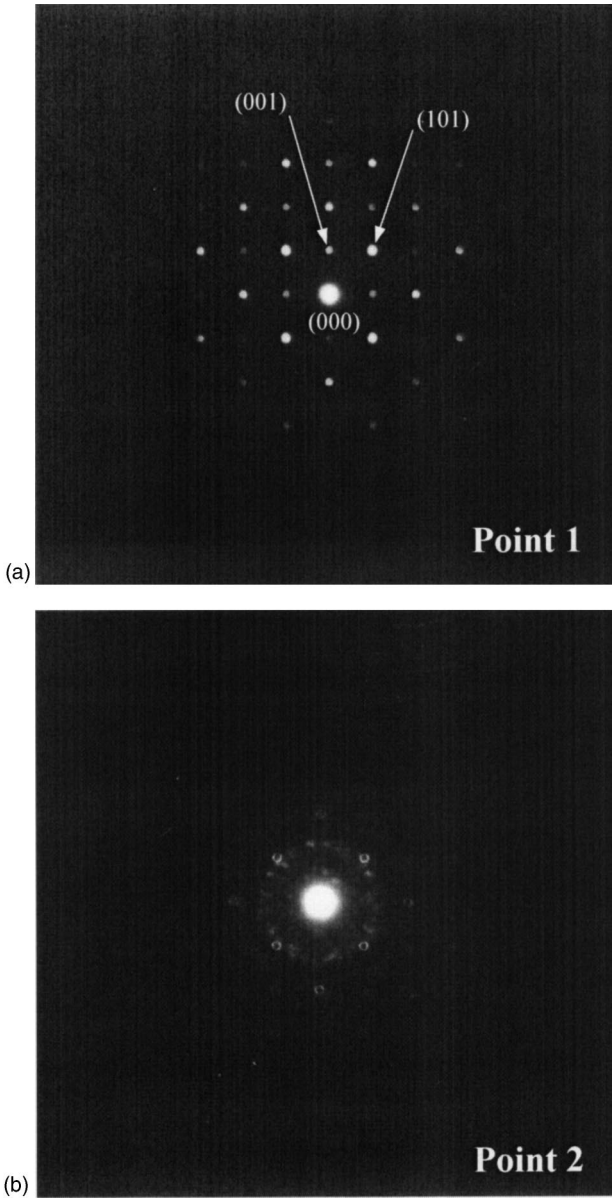

FIG. 9. (a) ED pattern of the point-1 well-crystallized area in Fig. 8. (b) ED pattern of the point-2 amorphouslike area in Fig. 8.

from the ED pattern and the HRTEM image, point 5 seems to be intermediate phase between point 3 and point 5. Moreover, there were visible Moiré fringes, suggesting that the two crystals overlap. The long period of Moiré fringes was approximately 13–14 nm, and also diffraction can be seen near (000) in the ED pattern. Interestingly, the direction of the Moiré fringes was found to be limited to either vertical or horizontal directions to substrate. The ED measurements clarified that the difference between the two Moiré fringes is due to the 90° rotation of the crystal structures of segregated phases. The preferential orientation of the nanoclustering along with the perovskite matrix can be rigorously understood in terms of lattice matching of either $(220)_{CeO_2} \| (002)_{perovskite}$ or $(220)_{CeO_2} \| (200)_{perovskite}$, where the lattice spacing of $(220)_{CeO_2}$ and $(002)_{perovskite}$ and/or $(200)_{perovskite}$ are 1.91 and 1.96 Å, respectively.

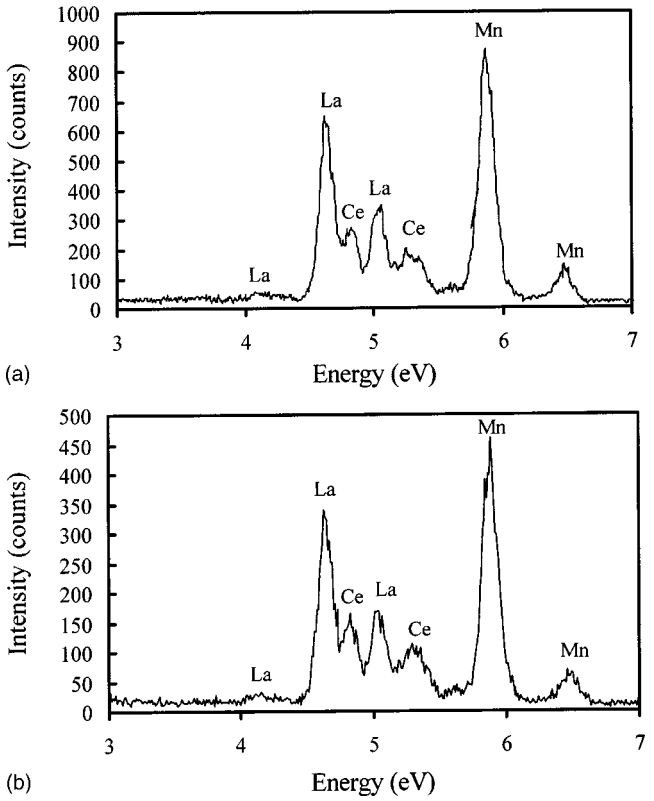

FIG. 10. (a) EDS data of the point-1 well-crystallized area in Fig. 8. (b) EDS data of the point-2 amorphouslike area in Fig. 8.

Here one can readily imagine that the third scenario based on nanoclustering cerium oxides could be acceptable as a reasonable interpretation if there were composition differences between the three phases. Figure 13 shows the EDS data of the three phases. A significant difference between the major compositions of each phase was found. The major compositions for point 3 are La and Mn, whereas point 4 is comprised of mainly Ce. In addition, quantitative evidence to prove the composition difference is shown in Table II. As to the drastic change of the phase transition temperatures due to post-annealing (Fig. 4), which was ranged from 150–300 K, it is also comparable to Curie temperature variations of La-deficient compositions $La_{1-x}MnO_3$ systems reported by Dezanneau *et al.*[30] since the origin is considered to be similar. Thus increasing the post-annealing temperature enhances gradually nanoclustering of cerium oxides due to thermal stabilization, reflecting the systematic variation of the phase transition temperature—see Fig. 4. Ultimately at the end of the annealing process under high temperature (800 °C), the primary phase of the film is almost $La_{1-x}MnO_3$ without Ce as shown in Fig. 13. The inset of Fig. 3(b) shows the magnetic

TABLE I. Averaged atomic cation ratio of as-grown films.

	Atomic ratio (%)		
	La	Mn	Ce
Point 1	36.21	49.26	14.53
Point 2	36.14	44.52	19.34

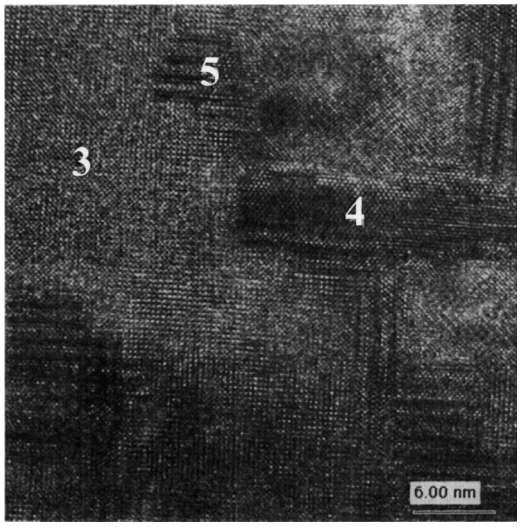

FIG. 11. High-resolution TEM image of $La_{0.7}Ce_{0.3}MnO_3$ thin film post-annealed at 800 °C under oxygen atmosphere.

moments at 10 000 Oe from M-H data measured at 10 K. The magnetic moment values for both as-grown and annealed films ranged from 2 to 2.5. Since the magnetic moment of the electron-doped system should be ideally ranged from 4 to 5 ($4.29\mu_B$ in theoretical calculation[34]), the measured values are obviously far below expected values for the electron-doped systems. In addition, the observed small magnetic moment compared with ideal values of electron-doped systems may indicate that the ferromagnetism of films is related to existing holes (ferromagnetic clusters) within material due to microstructural deficiencies, as reported by Topfer and Goodenough[28] in the case of $LaMnO_{3+\delta}$ systems. These experimental results highlight that any post-annealing should be avoided to realize the electron-doped systems due to thermal stabilization of Ce. Considering general trends on fabrication of electron-doped systems, it would be crucial to realize the electron-doped systems at the reduction atmosphere without any post-annealing. Although the HRTEM analysis indicated the presence of CeO_2 nanoclusters for O_2-annealed film, this could be also true for Ar-annealed films since the MI transition, FM transition, and Hall effect measurement data are totally comparable to the O_2-annealed sample. Although both oxygen and argon atmosphere post-annealing were performed in this study, the final oxygen composition of the films was not feasible to be measured. The film composition with the nonstoichiometry of oxygen composition is described as either $(La,Ce)MnO_{3-\delta}$ with oxygen vacancies or $(La,Ce)_{1-\varepsilon}MnO_3$ with cation vacancies. Since our physical interpretation for Ce-doped $LaMnO_3$ systems is based on the cation vacancies, it is noteworthy whether the presence of oxygen vacancies contradicts our interpretation or not. In the presence of oxygen vacancies, compensating the oxygen vacancies enhances hole doping in the case of hole-doped systems or decreases electron carriers in the case of electron-doped systems. Therefore the presence of oxygen vacancies does not change our physical interpretation for Ce-doped $LaMnO_3$ thin-film systems, which showed hole-type behavior. Although in a manner similar to $La_{1-x}MnO_3$ systems *A*-site cation deficiencies certainly result

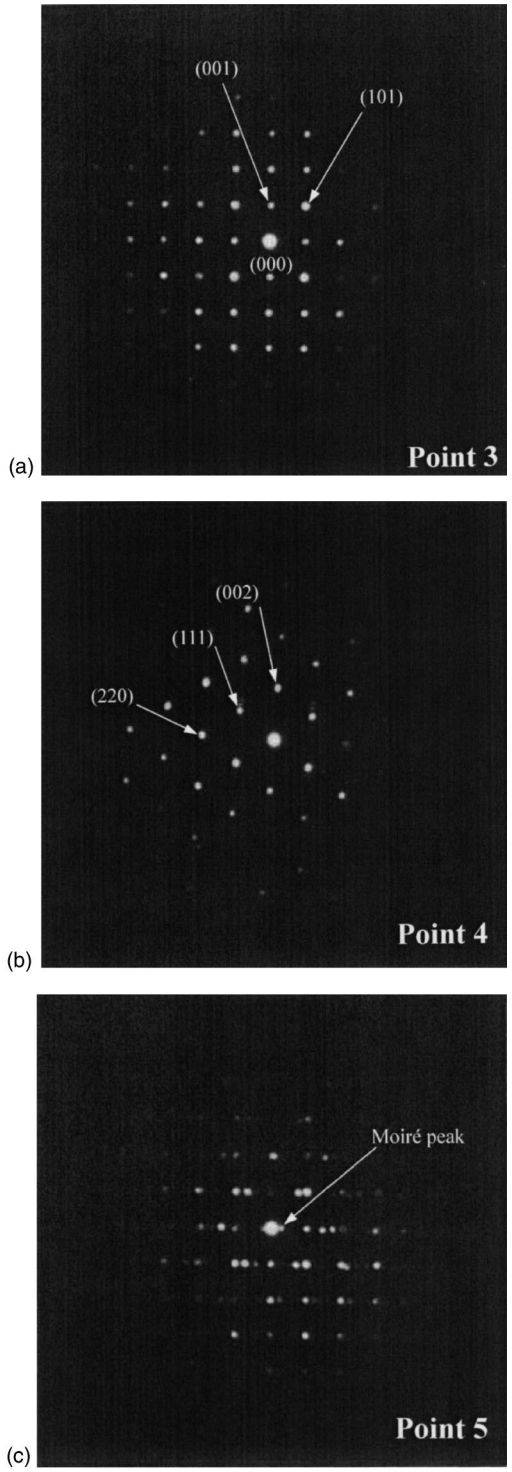

FIG. 12. (a) ED pattern of point 3 in Fig. 11. (b) ED pattern of point 4 in Fig. 11. (c) ED pattern of point 5 in Fig. 11.

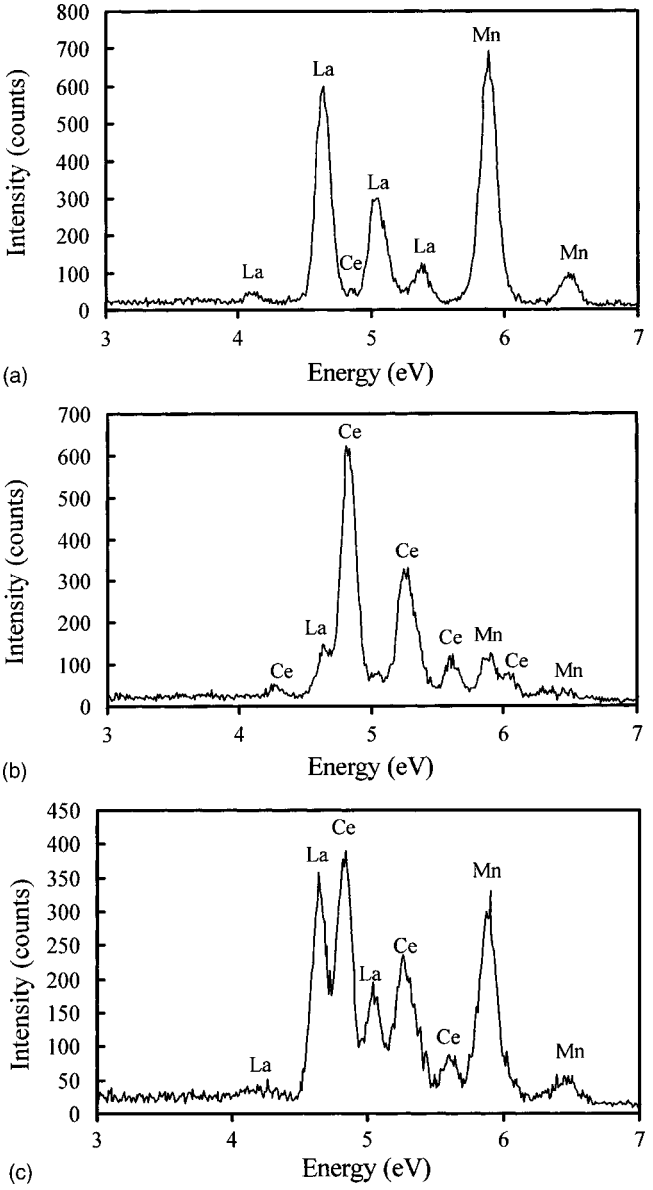

FIG. 13. (a) EDS data of point 3 in Fig. 11. (b) EDS data of point 4 in Fig. 11. (c) EDS data of point 5 in Fig. 11.

in the valence state of Mn^{4+}, we have not shown experimental results regarding the electric configurations in this paper. Considering the results of TEM-EDS, the valence state of Mn within our films may be a mixture of Mn^{2+}, Mn^{3+}, and Mn^{4+}. It is noted that the valence state of Mn is very sensitive to the degree of Ce ion segregation for $(La,Ce_{1-\delta})MnO_3$ systems. For instance, oversegregation from one-fourth of doped Ce ions in the *A* site drives the averaged valence state of Mn from Mn^{3+} into Mn^{4+} even in the presence of Ce^{4+}. Joseph Joly *et al.* also discussed that the ionic radius of Ce^{4+} ion is so small (0.97 Å) that the perovskite structure with Ce^{4+} would be unstable crystallographically. [The tolerance factor $t=(r_A+r_O)/\sqrt{2}(r_B+r_O)$ is 0.843.] Therefore, Mn^{3+},

TABLE II. Averaged atomic cation ratio of films post-annealed at 800 °C under oxygen atmosphere.

	Atomic ratio (%)		
	La	Mn	Ce
Point 3	46.90	51.67	1.43
Point 4	9.13	11.08	79.79
Point 5	29.72	29.12	41.16

Mn^{2+} (by Ce^{4+} doping), and Mn^{4+} (by Ce ion defect from the *A* site) ions may coexist in our annealed films. Judging from Hall measurement data and their relationship to T_{MI} (T_c), hole doping essentially contributes to metal-insulator (ferromagnetic-paramagnetic) transition phenomena. In other words, the spin moment of Mn^{4+} would behave ferromagnetically, while that of Mn^{2+} does not always behave ferromagnetically. Since information in the context with only the electric configurations—i.e., the valence state of manganese ions—is not conclusive to decide the origin of ferromagnetism of (La,Ce)MnO_3 systems, it would be an essential future work to investigate not only the electric configurations of manganese ions, but also their magnetic field dependence using x-ray magnetic circular dichroism (X-MCD).

As the interpretation of the nature of the metal-insulator and paramagnetic-ferromagnetic transition phenomena in our Ce-doped $LaMnO_3$ systems, the experimental results presented here strongly support the third scenario based on nanoclustering cerium oxides, which results in a mixture of *A*-site cation-deficient compositions $(La,Ce_{1-\delta})MnO_3$ and CeO_2 phases. Although our microstructural study showed the biphasic structure with nanoclustering CeO_2, it is the nature of Ce-doped $LaMnO_3$ films even in the absence of impurity peaks on the XRD data. We hope that the knowledge obtained in this study will contribute to the understanding of the physics of Ce-doped $LaMnO_3$ films and their properties.

IV. CONCLUSIONS

The nature of the phase transition phenomena of $La_{0.7}Ce_{0.3}MnO_3$ thin films with post-annealing was systematically investigated. The phase transition temperature was found to be significantly influenced by the post-annealing conditions and increases with increasing the post-annealing temperature in both oxygen and argon atmosphere annealing. Hall effect measurements identified the major carriers within the post-annealed films to be holes. Microstructural and composition analysis using TEM-EDS clarified that cation deficiencies due to nanoclustering cerium oxides within the films are responsible for the emergence of the metal-insulator transition and ferromagnetism phenomena.

ACKNOWLEDGMENTS

The authors would like to thank the Ministry of Education, Culture, Sports, Science and Technology of Japan for funding and supporting this project through the Center of Excellence (COE) program. Three of the authors (T.Y., T.K., and B.V.) acknowledge financial support from the Japan Society for the Promotion of Science (JSPS). The authors also acknowledge Dr. Kanai for fruitful suggestions.

*Corresponding author. Electronic address: kawai@sanken.osaka-u.ac.jp

[1] A. Urushiba, Y. Morimoto, T. Arima, A. Asamitsu, G. Kido, and Y. Tokura, Phys. Rev. B **51**, 14 103 (1995).
[2] H. Y. Hwang, S.-W. Cheong, P. G. Radaelli, M. Marezio, and B. Batlogg, Phys. Rev. Lett. **75**, 914 (1995).
[3] T. Kanki, H. Tanaka, and T. Kawai, Solid State Commun. **114**, 267 (2000).
[4] T. Kanki, H. Tanaka, and T. Kawai, Phys. Rev. B **64**, 224418 (2001).
[5] T. Kanki, H. Tanaka, and T. Kawai, J. Appl. Phys. **93**, 4718 (2003).
[6] T. Kanki, L. Run-Wei, Y. Naitoh, H. Tanaka, T. Matsumoto, and T. Kawai, Appl. Phys. Lett. **83**, 1184 (2003).
[7] T. Kanki, Y. G. Park, H. Tanaka, and T. Kawai, Appl. Phys. Lett. **83**, 4860 (2003).
[8] H. Tanaka, J. Zhang, and T. Kawai, Phys. Rev. Lett. **88**, 027204 (2002).
[9] J. Zhang, H. Tanaka, T. Kanki, J.-H. Choi, and T. Kawai, Phys. Rev. B **64**, 184404 (2001).
[10] P. Mandal and S. Das, Phys. Rev. B **56**, 15 073 (1997).
[11] J. R. Gebhardt, S. Roy, and N. Ali, J. Appl. Phys. **85**, 5390 (1999).
[12] C. Mitra, P. Raychaudhuri, J. John, S. K. Dhar, A. K. Nigam, and R. Pinto, J. Appl. Phys. **89**, 524 (2001).
[13] C. Mitra, P. Raychaudhuri, G. Kobernik, K. Dorr, K.-H. Muller, L. Schultz, and R. Pinto, Appl. Phys. Lett. **79**, 2408 (2001).
[14] P. Raychaudhuri, S. Mukherjee, A. K. Nigam, J. John, U. D. Vaisnav, R. Pinto, and P. Mandal, J. Appl. Phys. **86**, 5718 (1999).
[15] C. Mitra, P. Raychaudhuri, K. Dorr, K.-H. Muller, L. Schultz, P. M. Oppener, and S. Wirth, Phys. Rev. Lett. **90**, 017202 (2003).
[16] C. Mitra, Z. Hu, P. Raychaudhuri, S. Wirth, S. I. Csiszar, H. H. Hsieh, H.-J. Lin, C. T. Chen, and L. H. Tjeng, Phys. Rev. B **67**, 092404 (2003).
[17] S. Dai, Z. W. Li, A. H. Morrish, X. Z. Zhou, J. G. Zhao, and X. M. Xiong, Phys. Rev. B **55**, 14 125 (1997).
[18] Z. W. Li, A. H. Morrish, and J. Z. Jiang, Phys. Rev. B **60**, 10 284 (1999).
[19] J. Gao, S. Y. Dai, and T. K. Li, Phys. Rev. B **67**, 153403 (2003).
[20] G. T. Tan, S. Y. Dai, P. Duan, Y. L. Zhou, H. B. Lu, and Z. H. Chen, J. Appl. Phys. **93**, 5480 (2003).
[21] G. T. Tan, P. Duan, S. Y. Dai, Y. L. Zhou, H. B. Lu, and Z. H. Chen, J. Appl. Phys. **93**, 9920 (2003).
[22] J. Philips and T. R. N. Kutty, J. Phys.: Condens. Matter **11**, 8537 (1999).
[23] R. Ganguly, I. K. Gopalakrishnan, and J. V. Yakhmi, J. Phys.: Condens. Matter **12**, L719 (2000).
[24] V. L. Joseph Joly, P. A. Joy, and S. K. Date, J. Magn. Magn. Mater. **247**, 316 (2002).
[25] Y. G. Zhao, R. C. Srivastava, P. Fournier, V. Smolyaninova, M. Rajeswari, T. Wu, Z. Y. Li, R. L. Greene, and T. Venkatesan, J. Magn. Magn. Mater. **220**, 161 (2000).
[26] P. Murugavel, J. H. Lee, J. G. Yoon, T. W. Noh, J. S. Chung, M. Heu, and S. Yoon, Appl. Phys. Lett. **82**, 1908 (2003).
[27] T. Yanagida, T. Kanki, B. Vilquin, H. Tanaka, and T. Kawai, Solid State Commun. **129**, 785 (2004).
[28] J. Topfer and J. B. Goodenough, J. Solid State Chem. **130**, 117

(1997).
[29] L. Sudheendra, A. R. Raju, and C. N. R. Rao, Inter. J. Inorg. Mater. **2**, 657 (2000).
[30] G. Dezanneau, O. Isnard, H. Roussel, A. Sin, M. Audier, and H. Vincent, Cryst. Eng. **5**, 347 (2002).
[31] J. C. Chen, S. C. Law, L. C. Tung, C. C. Chi, and W. Guan, Phys. Rev. B **60**, 12 143 (1999).
[32] S. H. Chun, M. B. Salamon, Y. Lyanda-Geller, P. M. Goldgart, and P. D. Han, Phys. Rev. Lett. **84**, 757 (2000).
[33] H. C. Yang, L. M. Wang, and H. E. Horng, Phys. Rev. B **64**, 174415 (2001).
[34] Q. Zhang and W. Zhang, Phys. Rev. B **68**, 134449 (2003).